Japan J. Indust. Appl. Math.
DOI 10.1007/s13160-015-0195-3

ORIGINAL PAPER

Area 3

Neuromechanical pumping: boundary flexibility and traveling depolarization waves drive flow within valveless, tubular hearts

Austin Baird[1] · **Lindsay Waldrop**[2] · **Laura Miller**[3]

Received: 18 August 2015 / Revised: 4 October 2015

Abstract In this paper, we develop a neuromechanical model of pumping in a valveless, tubular heart inspired by the tunicate, *Ciona savignyi*. Valveless, tubular hearts are common throughout the animal kingdom. The vertebrate embryonic heart first forms as a valveless, tubular pump. The embryonic, juvenile, and adult hearts of many invertebrates are also valveless, tubular pumps. Several different pumping mechanisms have been propsed for tubular hearts, and it is not clear if all animals employ the same mechanism. We compare the flows generated by this pumping mechanisms to those produced by peristalsis using a prescribed contraction wave and to those produced by impedance pumping across a parameter space relevant to *Ciona savignyi*. The immersed boundary method is used to solve the fully-coupled fluid-structure interaction problem of an elastic tubular heart immersed in a viscous fluid. The FitzHugh–Nagumo equations are used to model the propagation of the action potential which initiates the contraction. We find that for the scales relevant to *Ciona*, both the neuromechanical pumping mechanism and peristalsis produce the strong flows observed in the tunicate heart. Only the neuromechanical model produces flow patterns with all of the characteristics reported for valveless, tubular hearts. Namely, the neuromechanical pump generates a bidirectional wave of contraction and peristalsis does not.

✉ Laura Miller
lam9@unc.edu

Austin Baird
ajbaird86@gmail.com

Lindsay Waldrop
lwaldrop@ucmerced.edu

[1] 2015 Sunset Ave, Durham, NC 27705, USA

[2] School of Natural Sciences, 5200 N. Lake Rd., Merced, CA 95343, USA

[3] CB 3250 Phillips Hall, Chapel Hill, NC 27599, USA

Keywords Tubular hearts · Peristalsis · Liebau pumping · Immersed boundary method · FitzHugh–Nagumo · Embryonic hearts · Tunicates

Mathematics Subject Classification 92C35

1 Introduction

Valveless, tubular hearts that drive fluid flow within or through enclosed spaces are widespread in the animal kingdom (reviewed by Xavier-Neto et al. [31]). Among other functions, these pumps are important for driving flow within circulatory and/or respiratory systems (e.g. [7,18,21,22,26]).

Both impedance pumping and peristalsis have been proposed as mechanisms by which tubular hearts drive flow [6,17,30]; this question is unresolved [17]. Impedance pumping occurs when a single point of contraction produces passive, elastic waves that propagate bidirectionally along an elastic section of tube with rigid ends. This mechanism is characterized by a non-linear relationship between pumping frequency and volumetric flow rate [15,16]. Peak flow velocities may also exceed the speed of the contraction wave. Forouhar et al. [6] found these characteristics of flow produced by the vertebrate embryonic heart at the tubular stage, leading them to conclude that impedance pumping was at work within these hearts. Another characteristic of impedance pumps is that the flow direction is not determined by a morphological feature (e.g. one-way valve), but by the orientation of the compression site relative to the rigid section of tube, the rigidity of the elastic section, and the pumping frequency. Note that such flow reversals were not observed in their study.

Prior to Forouhar's paper, the contractions of tubular hearts were described as peristaltic. Peristalsis is defined as a wave of active contraction that propagates down the length of a tube. Flow direction is determined by the direction of the propagating wave. Peristalsis is traditionally modeled using a prescribed wave of contraction that removes coupling between the fluid and the elastic structure. Using this approach, passive, elastic waves are not observed or incorporated. Flow speeds produced by peristalsis typically yield a linear relationship with pumping frequency as long as the wave speed changes proportionally with the frequency [6,17]. Recent work has shown that a non-linear relationship can be obtained by decoupling pumping frequency from the speed of the contraction wave [30]. Peak flow speeds may also exceed the wave speed if the contraction amplitude is sufficiently large so as to nearly occlude the tube [25]. By modeling peristalsis using a prescribed unidirectional contraction wave, some of the phenomena observed in actual hearts, such as a bidirectional contraction wave, are not captured.

When exploring various pumping mechanisms, it is important to consider the scale relevant to the problem. Tubular hearts and other tubular pumps drive fluid over a large range of tube diameters (L) and pumping frequencies (ω), and the combination of these variables matters substantially to subsequent fluid flow produced. A dimensionless number that describes the relative importance of unsteady effects is the Womersley number (Wo),

$$Wo = L\sqrt{\frac{\omega}{\nu}} \tag{1}$$

where ν is the kinematic viscosity of the fluid being driven. For $Wo >> 1$, viscous effects are negligible. For $Wo < 1$, viscosity dampens out the inertia of pulsatile pumping mechanisms, reducing their efficacy. In the case of pumping in elastic tubes, the relative effect of viscosity (which is proportional to the Wo) and the stiffness of the heart wall determine whether or not passive elastic waves will emanate from the actuation point. If viscous effects are large relative to the stiffness, the system is overly damped. Baird et al. [2] observed that little to no net flow was generated by impedance pumping for the stiffnesses considered for $Wo \approx 1$, a case in which the system was overly damped with no passive, elastic waves of contraction. This result was also predicted by an analytical model described by Bringley et al. [3]. When active traveling waves are prescribed for peristalsis, significant flow was generated for Wo well below 1 [2,29,30].

Since tubular hearts can share several of these features, we propose a pumping mechanism that combines aspects of both traditional peristalsis and impedance pumping: bidirectional traveling waves of active contraction of an elastic boundary that is fully coupled to the fluid. This mechanism is based on observations of the tubular, valveless heart of tunicates (Chordata: Tunicata). Tunicates are the closest invertebrate relatives to vertebrates and are used as a model organism for molecular heart development [4,14,32]. Furthermore, tunicates come in a wide variety of sizes with hearts that span important transitional ranges of $0.1 < Wo < 10$.

The tunicate heart consists of a myocardium which is enclosed by a pericardium, both tissues are one cell layer thick and are separated by a fluid-filled intrapericardial space [11]. The pericardium is stiff and provides structural support to the myocardium [29]. The myocardium, connected to the the pericardium only at a line that runs down the length of the heart tube, consists of a single, flexible layer of myoepithelial contractile cells which contract to reduce the diameter of the inner lumen [1,11,13]. Muscle fibers wind around the entire length of the heart tube, and traveling action potentials that initiate contraction have also been measured along the entire length [1,13]. Myocardial contractions begin at pacemaker regions at either ends of the heart tube; one pacemaker causes local depolarization of myocardial cells which propagates down the contractile region of the heart tube. The propagation of action potentials may occur in either direction.

The neuromechanical pumping mechanism models the basic kinematics of pumping by tunicate hearts by using the FitzHugh–Nagumo equations to model the activation-signal propagation. The activation signal propagates down the heart tube and initiates an applied force (acting as the muscle) that reduces the diameter of the heart tube. The immersed boundary method (IBM) is used to model the interactions of this traveling wave of applied force, the flexible boundary of the heart tube, and the coupled interactions between the flexible structure and the surrounding fluid. Each simulation includes a stiff boundary enclosing the heart tube (a pericardium) to provide structural support to the contracting region.

In this study, we investigate flow produced by the neuromechanical pumping model for the parameter space relevant to the tunicate, *Ciona savignyi*. We compare the performance of the neuromechanical pumping model to models of traditional peristalsis and impedance pumping at a range of Wo and pumping frequencies for conduction velocities that are both coupled to pumping frequency and constant.

2 Methods

2.1 Immersed boundary method

The equations describing an elastic heart driving a viscous fluid were solved using the immersed boundary method. The immersed boundary method was first developed by Peskin [23] to simulate cardiac flows in the adult human heart, and this method provides a relatively straightforward approach for solving fully-coupled fluid-structure interaction problems. Since its original development, a number of other methods have been used to handle the fully-coupled fluid structure interaction problem in a similar way [20]. The method works well at a variety of scales found below the turbulent regime, making it useful in many biological applications. Some of these applications include swimming organisms in viscoelastic fluids [27], insect flight [19], and lamprey swimming [28].

The immersed boundary method handles the problem of having an elastic boundary immersed in an incompressible viscous fluid by using two separate but interactive coordinate frames. The incompressible fluid is discretized on a fixed Cartesian grid (Eulerian frame) and the elastic boundary is discretized on a moving curvilinear mesh (Lagrangian frame). The deformation of the boundary generates a force which is imparted to the surrounding fluid. The fluid is then driven by this force, and the boundary moves at the local fluid velocity.

The governing equations for the fluid are defined by the full, 2D Navier–Stokes equations given as

$$\rho\left(\frac{\partial \mathbf{u}}{\partial t}+\mathbf{u}\cdot\nabla\mathbf{u}\right)=-\nabla p(\mathbf{x},t)+\mu\nabla^2\mathbf{u}+\mathbf{f}(\mathbf{x},t), \tag{2}$$

$$\nabla\cdot\mathbf{u}=0. \tag{3}$$

where μ is the dynamic viscosity defined as $\nu\rho$, ρ is the density of the fluid, p is the pressure, and $\mathbf{u}$ is the velocity of the fluid. Equation 2 is the momentum equation for a fluid, and Eq. 3 defines the incompressibility of a constant density fluid.

The body force, $\mathbf{f}(\mathbf{x}, t)$ is particular to the application and may include resistance to bending, resistance to stretching, displacement from a tethered position, the action of virtual muscles, or external forces [23]. One of the simplest types of force is a penalty force that is proportional to the displacement of the immersed boundary from a target or preferred position. This target position could be fixed or move with a prescribed motion. The position in Cartesian coordinates of the immersed boundary that interacts with the fluid is given by $\mathbf{X}(s, t)$. Here s describes the position of a point on the boundary along its length. To move the boundary in a preferred motion, the positions of the target points are described using Cartesian coordinates that may change in time as defined by $\mathbf{Y}(s, t)$. When the immersed boundary points deviate from the preferred position, a force is applied that is proportional to the distance between the target and actual boundaries. This force can be adjusted by changing the magnitude of k_{target} so that the distance between the actual boundary and its preferred configuration is kept within some tolerance. The force that results follows Hooke's law and is defined to be:

$$\mathbf{F}_{target}(s,t) = k_{target}(\mathbf{Y}(s,t) - \mathbf{X}(s,t)). \tag{4}$$

Note that this method was used to move sections of the boundary in a prescribed motion for the peristalsis and valveless pumping models described below.

In addition to the target force, forces may also be generated through the elastic properties of the boundary. For this application, every boundary point along the heart tube is connected by a series of beams and springs that resist bending and stretching, respectively. These additional forces can be calculated as

$$\mathbf{F}_{beam}(s,t) = \kappa_{beam} \frac{\partial^4 \mathbf{X}(s,t)}{\partial s^4}, \tag{5}$$

$$\mathbf{F}_{spring}(s,t) = \kappa_{spring} \left\{ \left(\left| \frac{\partial \mathbf{X}(s,t)}{\partial s} \right| - 1 \right) \frac{\partial \mathbf{X}(s,t)/\partial s}{|\partial \mathbf{X}(s,t)/\partial s|} \right\}. \tag{6}$$

Equation 5 is the beam equation which describes the force generated due to the resistance to bending, and κ_{beam} is the corresponding coefficient of stiffness. Equation 6 describes the force resulting from the tube's resistance to stretching and compression, and κ_{spring} is the corresponding spring coefficient. A summation of all three forcing terms is then used to describe the total force applied to the fluid due to the boundary. This force is defined to be

$$\mathbf{F}(s,t) = \mathbf{F}_{target}(s,t) + \mathbf{F}_{beam}(s,t) + \mathbf{F}_{spring}(s,t). \tag{7}$$

To spread this force to the surrounding fluid discretized on a Cartesian grid and to move the boundary at the local fluid velocity, Eqs. 2 and 3 are coupled to the boundary equations using integral transforms with delta function kernels:

$$\mathbf{f}(\mathbf{x},t) = \int \mathbf{F}(s,t)\delta(\mathbf{x} - \mathbf{X}(s,t))ds \tag{8}$$

$$\frac{\partial \mathbf{X}}{\partial t} = \mathbf{u}(\mathbf{X}(s,t),t) = \int \mathbf{u}(\mathbf{x},t)\delta(\mathbf{x} - \mathbf{X}(s,t))d\mathbf{x}. \tag{9}$$

To numerically approximate these integral transforms, a regularized delta function, δ_h, is used,

$$\delta_h(\mathbf{x}) = \frac{1}{h^2}\phi\left(\frac{x}{h}\right)\phi\left(\frac{y}{h}\right), \tag{10}$$

where $h = dx$ is the numerical mesh width. Here we can define $\phi(r)$ as

$$\phi(r) = \begin{cases} \frac{1}{4}(1+\cos(\frac{\pi r}{2})) & |r| \leq 2 \\ 0 & otherwise \end{cases} \tag{11}$$

where r is the distance from the Lagrangian point. A more detailed discussion of such regularized delta functions may be found in [23]. The smoothed approximation to the force density is now defined in the Eulerian frame as $\mathbf{f}(\mathbf{x}, t)$. To numerically solve the fluid equations, Eqs. 2 and 3 are discretized on a periodic 630 × 630 grid and solved using a fast Fourier transform fluid solver, details of which can be found in [24]. Since most of the action is within the racetrack, the flow velocity is negligible at the boundary, and the periodicity has little effect on the results. Once the fluid velocity is calculated, a discretization of Eq. 9 with the regularized delta function is used to interpolate the local fluid velocity to the Lagrangian boundary points, and the boundary is moved at this velocity. This effectively enforces a no-slip condition at the boundary. Once the new position of the boundary is updated, one time-step of the immersed boundary routine is concluded.

2.2 Model set up

To investigate the three pumping mechanisms, a numerical model of the tube is constructed in two dimensions (not axisymmetric). For comparison with previous analytical, numerical, and experimental work, the computational immersed boundary will resemble a closed racetrack. The section of tube where the contraction occurs is flexible, and the remainder of the racetrack is relatively rigid, see Fig. 1. The racetrack is constructed by connecting two half circles to two straight portions of tube. These circles are off center with radii set so that the diameter of the channel is equal throughout. The circular sides and the top of the racetrack are tethered to target points so that they are relatively rigid.

For the neuromechanical and impedance models, the bottom straight portion of the racetrack resists bending and stretching with no tethered points so that the boundary

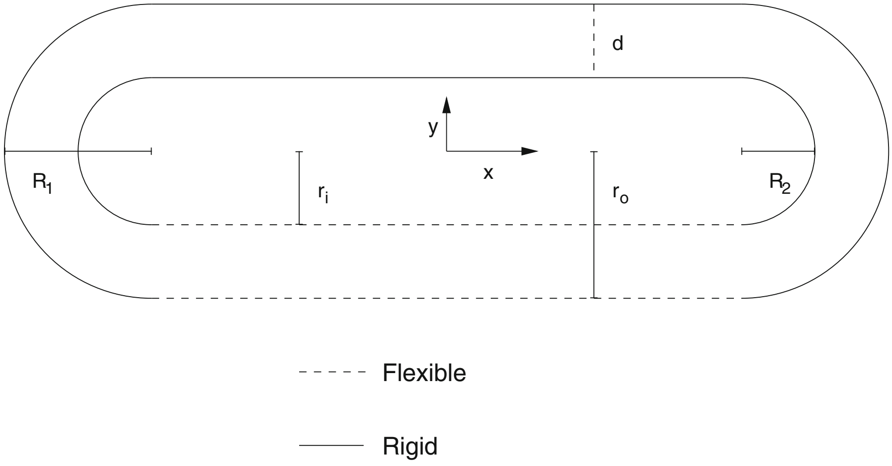

Fig. 1 Model of a closed valveless racetrack. *Dotted portions* identify flexible regions and *solid lines* indicate rigid regions. Pumping mechanics are implemented along the flexible section denoted by *dotted lines*. R_2 is the inner radius, R_1 is the outer radius, d is the diameter, r_i is the distance to the inner straight tube from the origin (and also the distance to the center of the offset circular regions), r_o is the distance from the origin to the outer straight portion of the tube

Table 1 Mechanical variables for the heart tube simulations

Parameter	Value
Density of the fluid $[\rho]$ $(\frac{kg}{m^3})$	1025
Viscosity of the fluid $[\mu]$ $(\frac{kg}{ms})$	Prescribed
Bending coefficient of the boundary $[\kappa_{beam}]$ (Nm^2)	3.24×10^6
Stretching stiffness of the boundary $[\kappa_{spring}]$ $(\frac{kg}{s^2})$	3.24×10^6
Stretching stiffness of target points $[\kappa_{target}]$ $(\frac{kg}{s^2})$	3.24×10^6

Table 2 Non-dimensional parameter values used for solving the FitzHugh Nagumo equations and constructing the pericardium

Parameter	Value
Threshold potential $[a]$	0.1
Strength of blocking $[\epsilon]$	0.1
Diffusion coefficient $[\mathcal{D}]$	30–220
Resetting rate $[\gamma]$	0.5
Current injection $[\mathcal{I}]$	0.5
freq $[f]$ (Hz)	0.1–2.1

Parameters were tuned to match the dynamics of the tunicate heart

can move freely. For the peristaltic model, the bottom of the racetrack is also connected to tethered points that move with a prescribed motion. To describe the curved regions of the tube, we define the inner radius to be R_2, the outer radius to be R_1, and the horizontal shift as r_i, see Fig. 1. The half circles are constructed by setting the (x, y) coordinates as

$$(x, y) = \begin{cases} (R_2 \cos(\theta),\ R2 \sin(\theta) \pm r_i)\ r = R_2 \\ \\ (R_1 \cos(\theta),\ R_1 \sin(\theta) \pm r_i)\ r = R_1 \end{cases} \tag{12}$$

with the ± indicating which side of the tube you are describing. Note that the horizontal shift is the same distance as to the bottom straight tube. Also note that $\theta \in (-\frac{3\pi}{2}, \frac{\pi}{2})$ for the right hand portion of the tube and $\theta \in (\frac{\pi}{2}, -\frac{3\pi}{2})$ for the left hand portion. The racetrack is immersed in a incompressible viscous fluid with constant density, ρ. For the Wo sweeps where frequency is kept constant, the dynamic viscosity, μ, is adjusted to obtain the correct Wo. Relevant physical and numerical parameters are summarized in Tables 1 and 2.

2.3 Pumping mechanisms

2.3.1 Neuromechanical model

The neuromechanical model combines the characteristics of previous models of valveless, tubular pumping, namely: active waves of contraction along an elastic tube and bidirectional, passive, elastic waves. As motivation for the inclusion of active waves of contraction we note that traveling actions potentials have been recorded in the hearts of *Ciona intestinalis* (a sister species to *Ciona savignyi*) in previous studies by [13]. These traveling action potentials are known to activate the muscular fibers that run the length of the heart tube. A complete mathematical model of the tunicate heart should then incorporate both the fluid dynamics, elastic properties of the tube, and the activation of contractile muscles along its length.

To begin modeling this system, we first need to describe how to best model traveling action potentials in a heart tube. The Hodgkin–Huxley equations were the first quantitative model of propagation of an electrical signal along excitable cells, such as the excitable myocardial cells found in the tunicate heart [9]. The essential dynamics of this model have since been captured by the reduced order FitzHugh–Nagumo equations [5]. The dimensionless form is given by:

$$\frac{\partial v}{\partial t} = \mathcal{D}\nabla_x v + v(v-a)(v-1) - w - \mathcal{I}(t) \tag{13}$$

$$\frac{\partial w}{\partial t} = \epsilon(v - \gamma w), \tag{14}$$

where $\mathcal{D}$ = diffusion rate of potential, $v(x,t)$ = membrane potential, $w(x,t)$ = blocking mechanism, a = threshold potential, γ = resetting rate, ϵ strength of blocking, and the applied current $\mathcal{I}(t)$, which is a function of time, t. Here v represents the fast variable (potential) and w represents the slow variable (sodium channel blocking), the kinetics of which are controlled by the parameter: $\epsilon << 1$. Phase portraits of this non-linear system have been shown to capture many salient dynamical properties of cardiomyocytes [12].

To couple the applied force that drives the movement of the boundary to the electropotential given by the FitzHugh–Nagumo equations, please refer to Fig. 2. Along the elastic portion of the racetrack, springs with variable stiffness are connected to the top and bottom of the elastic section of tube. The stiffnesses are functions of the traveling electropotential which varies in time due to the current applied to the pacemaker

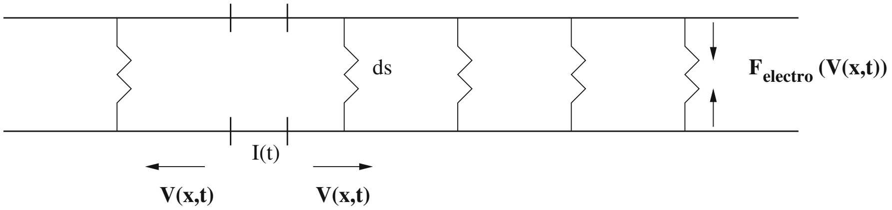

Fig. 2 This *diagram* shows our numerical model of the coupled dynamics problem. We attach springs to to the *top* and *bottoms* elastic walls of the tube and a force proportional to the traveling action potential, $F_{electro}(V(x,t))$. We then inject a current, $I(t)$, at a location of the pacemaker periodically throughout the simulation. The FitzHugh–Nagumo equations are solved along the tube walls to determine the electropotential at each position and at each time. The force is generated by changing the stiffness of these springs, and results in contractions down the length of the tube wall

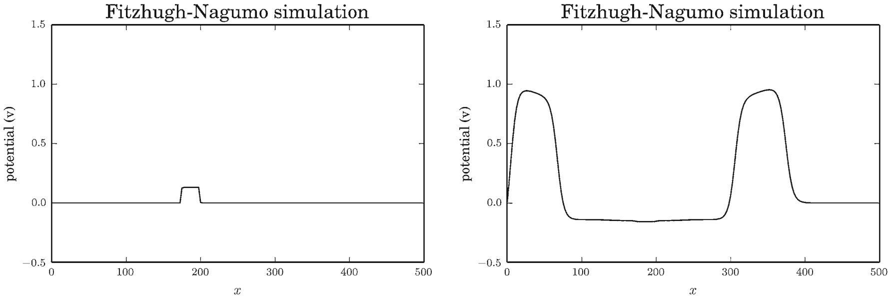

Fig. 3 The *figure* on the *left* shows an initial current begin initiated in the pacemaker region. The *figure* on the *right* shows the bi-directional propagation of the action potentials down the length of the domain. All parameters are dimensionless for this figure

region. At each time step we solve for these potentials by discretizing the FitzHugh Nagumo equations as follows:

$$v_i = v_{i-1} + dt_f \left(\mathcal{D} \left(\frac{v_i - 2v_{i-1} + v_{i-2}}{dx_f^2} \right) - v_{i-1}(v_{i-1} - 1)(v_{i-1} - a) - \omega_{i-1} + \mathcal{I}_i \right) \tag{15}$$

$$\omega_i = \omega_{i-1} + \epsilon dt_f (v_{i-1} - \gamma \omega_{i-1}). \tag{16}$$

Here we use a forward-Euler time-step integrator and a centered differencing scheme to represent the spatial diffusion operator. Dynamics of this system can be seen in Fig. 3. The other parameters are prescribed to capture the associated dynamics observed in the tunicate heart tubes. Time is scaled in order to match the dynamics of the generated action potentials to the desired active wave of contraction and is given by:

$$dt_f = \frac{dt\mathcal{F}}{\mathcal{T}}, \tag{17}$$

where $\mathcal{F}$ is a non-dimensional scaling parameter and $\mathcal{T}$ is the desired pumping period. The spatial location, x, is also scaled in order to match the desired dynamics of the active wave of contraction. Once we calculate the electropotential at a given point in space, we can determine a spring stiffness that is used to describe the action of the muscles at time t,

$$\kappa_e(x, t) = \kappa_m (v^4(x, t)). \tag{18}$$

In this simplified model of the muscle, κ_m is a scaled spring stiffness and $v(x, t)$ is the traveling action potential. This new spring stiffness is then used to determine the force generated by the springs that connect the bottom and top of the elastic tube, representing the action of the muscle. This phenomenological model has the effect of producing a wave of active contraction. Note that the passive elastic properties of the heart tube, κ_{beam} and κ_{spring}, do not change in time. The value of κ_m is tuned to produce the amount of contraction observed in *Ciona* hearts.

Table 3 Spatial dimensions and numerical parameters for the heart tube simulations

Parameter	Value
Length of domain (m)	5.0×10^{-4}
Width of domain (m)	5.0×10^{-4}
Diameter of tube [d] (m)	3.5×10^{-5}
Outer radius [R_1] (m)	1.0×10^{-4}
Inner radius [R_2] (m)	R1—diameter
Distance to inner straight tube [r_i] (m)	1.25×10^{-4}
Distance to outer straight tube [r_o] (m)	1.25×10^{-4} + d
Length of straight tube (m)	2.5×10^{-4}
Frequency of pumping ($\frac{1}{s}$)	0.3–2.2
Womersley number [Wo]	0.3–16
Percent of contraction	0.8
Pulse Period (s)	1.0
Final simulation time (s)	8.0
Time step [dt] (s)	3.05×10^{-5}
Velocity output time step (s)	0.025
Spatial step [dx] (m)	8.33×10^{-7}
Boundary step [ds] (m)	4.17×10^{-7}

These are dimensional parameters used to simulate impedance pumping and peristalsis to investigate scaling effects on pumping efficacy

2.4 Simulation parameters and data analysis

Default parameters used for simulations are reported in Tables 3 and 1. The elastic properties chosen are within the range of those estimated for *Ciona* [29]. Note that for these dimensions and range of Wo, the dynamics of flow do not seem to depend significantly upon changes in material properties of the heart tube over a couple orders of magnitude [29]. Immersed boundary simulations of neuromechanical pumping and impedance pumping were conducted at a variety of Wo by varying the viscosity of the fluid. To compare the performance of the pumping mechanisms, the spatially averaged velocity is taken along a cross section of the diameter of the tube in a non-contracting region. These spatially averaged velocities are then temporally averaged across the pulses to determine the net flow as a function of Wo as well as the pumping frequency with viscosity held constant. These velocities are presented as non-dimensional numbers, calculated by dividing by a characteristic velocity defined to be: $\frac{d}{\mathcal{T}}$, here, d is the diameter of the computational model tube and $\mathcal{T}$ is the period of pumping. We also non-dimensionalized time by dividing by the pumping period.

2.4.1 Peristalsis and impedance pumping

To compare the flow produced by the neuromechanical pump, we will reference previously published data generated using models of peristalsis and impedance pumping that have been described and reported in [2].

To simulate peristalsis, the points of the contracting region of the tube are tethered and move with points that move by prescribed motion. The peristaltic wave is constructed from the following parts: the initial contraction, the translation of the contracted region, and decompression. The contraction begins on the left hand side of the straight tube and travels to the end of this section before the next wave begins.

The model of impedance pumping includes an isolated region of active contraction where the motion is generated by tethering those boundary points to target points that move with a preferred sinusoidal. This movement then generates passive elastic waves that travel down the elastic portion of the tube. The region of active contraction is off center, and its position affects the direction and magnitude of the flow. The actuation site used for impedance pumping coincided with the placement of the pacemaker used for neuromechanical pumping.

3 Results

3.1 Flow characteristics produced by neuromechanical pumping

We present a model of flow through a valveless, tubular heart that combines elements of impedance pumping and peristalsis. Specifically, this model includes a bidrectional traveling wave of active contraction originating at an off-center pacemaker that initiates the contraction of an elastic boundary. The pacemaker is modeled as a periodic applied current $\mathcal{I}(t)$ that triggers the propagation of action potentials along the heart tube, see Fig. 2. This is distinctly different from traditional impedance pumping because there is an active, rather than passive, traveling wave. It is also different from a traditional model of prescribed peristalsis in that the contraction is bidirectional and the resulting motion is due to the interaction of the active force generation, the elastic boundary, and the fluid.

Figure 4 shows a vorticity map, configuration of the elastic boundary, and the position of passive tracer particles during the first pulse for $t = \frac{\mathcal{T}}{4}, \frac{\mathcal{T}}{2}, \frac{3\mathcal{T}}{4}$, and $\mathcal{T}$. Note that the colormap used is normalized for all figures, so that the magnitude of vorticity can be directly compared between each case. The Wo was set to 1.0 and the frequency was set to 1 Hz. Figure 4a shows the contraction wave moving bidirectionally from the pacemaker region. In Fig. 4b, the contraction wave is reflected at the inflow tract and combines with the right traveling wave (Fig. 4c). At the end of the cycle, the passive tracer particles have been pushed beyond the outflow tract and into the rigid section of the racetrack. Note that the dynamics of the pump share many of the same qualities as those described for traditional impedance pumping.

3.2 A comparison of the three types of pumping mechanisms

To test the effects of the choice of pumping mechanism on flow generated by the tubular, valveless heart model, we also performed corresponding simulations for peristalsis and impedance pumping. For this comparison, the pumping frequency was set to 1 Hz for all cases. The Wo was set to 1 and was varied in the subsequent section by changing the dynamic viscosity, μ.

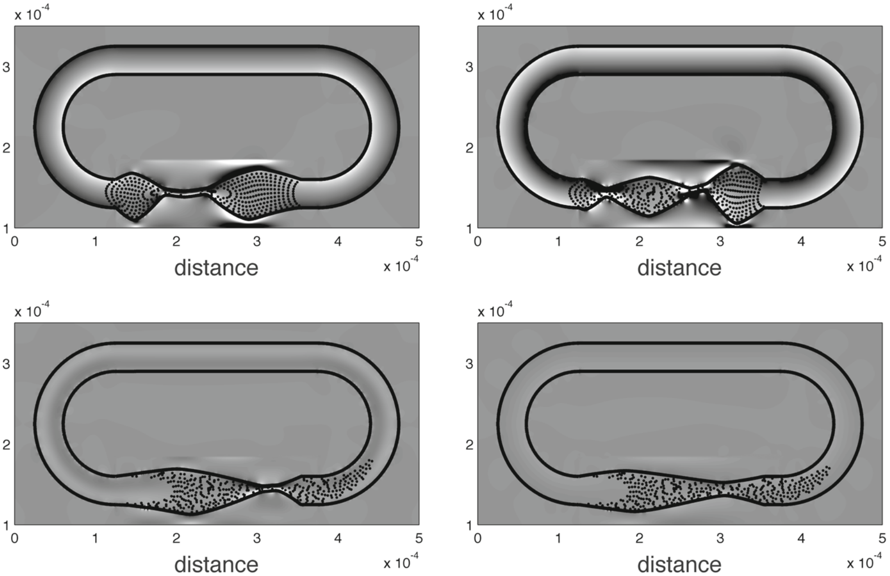

Fig. 4 Neuromechanical pumping during the first pulse cycle at $t = \frac{\mathcal{T}}{4}, \frac{\mathcal{T}}{2}, \frac{3\mathcal{T}}{4}$, and $\mathcal{T}$. The Wo was set to 1.0 and the frequency was set to 1 Hz. The *graymap* shows the vorticity, and the *black dots* are passive tracers that move at the local fluid velocity

Figure 5 shows the vorticity, position of the elastic boundary, and positions of the tracer particles during the first pulse of impedance pumping for $t = \frac{\mathcal{T}}{4}, \frac{\mathcal{T}}{2}, \frac{3\mathcal{T}}{4}$, and $\mathcal{T}$. The characteristic, passive traveling wave of the impedance pump is damped by the shear forces encountered from the high viscosity of the fluid. Passive tracer particles marking fluid flow in the tube show that the flow is close to reversible, resulting in very little net movement of the fluid. Impedance pumping appears to have limited to no efficacy at low Wo for this choice of elasticity and geometry.

Figure 6 shows the vorticity, position of the elastic boundary, and positions of the tracer particles during the first pulse using peristalsis for $t = \frac{\mathcal{T}}{4}, \frac{\mathcal{T}}{2}, \frac{3\mathcal{T}}{4}$, and $\mathcal{T}$. Fluid flows produced by peristalsis show steady, counter-clockwise flow at $Wo = 1,\ f = 1.0$ Hz. Figure 6a shows the intial contraction of the tube followed by the translation of the compression site (b, c). The contraction is relaxed at the end of the cycle (Fig. 6d). Flow profiles show an initial acceleration of fluid with the beginning of contraction, steady flow during translation of the contraction down the tube with flow decelerating when the contraction relaxes.

Figure 7 shows the dimensionless flow velocity averaged along a cross section in the rigid outflow tract vs. dimensionless time for each of the pumping mechanisms at $Wo = 1$ and $f = 1$. For these parameters, impedance pumping shows low amplitude oscillatory flows with little net transport. The fluid is pushed in the positive direction (counterclockwise) during contraction and is pulled in the negative (clockwise) direction during re-expansion. In the case of peristalsis, the fluid accelerates rapidly during the initial contraction, maintains a nearly constant speed during the translation of the contraction site, and rapidly decelerates during the re-expansion of the contraction site.

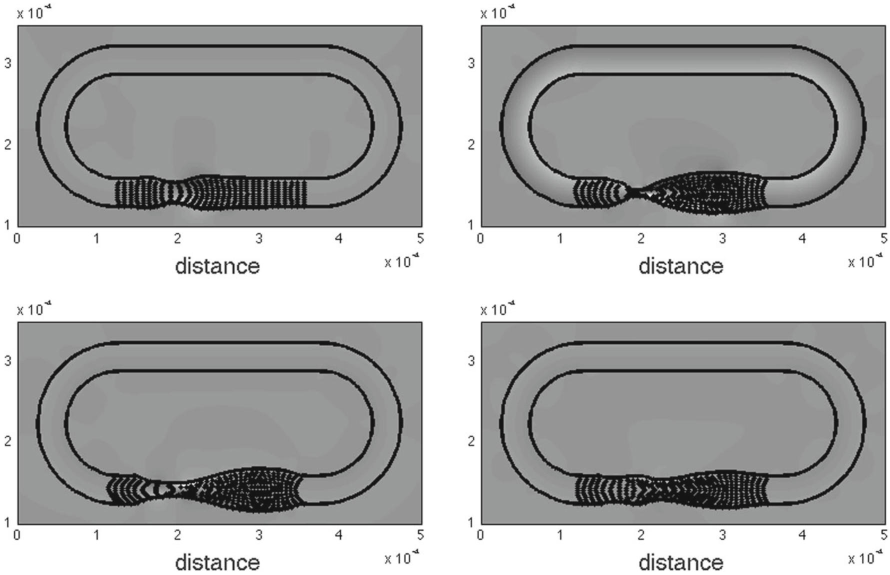

Fig. 5 Impedance pumping during the first pulse cycle at $t = \frac{\mathcal{T}}{4}, \frac{\mathcal{T}}{2}, \frac{3\mathcal{T}}{4}$, and $\mathcal{T}$. The Wo was set to 1.0 and the frequency was set to 1 Hz. The *graymap* shows the vorticity, and the *black dots* are passive tracers that move at the local fluid velocity

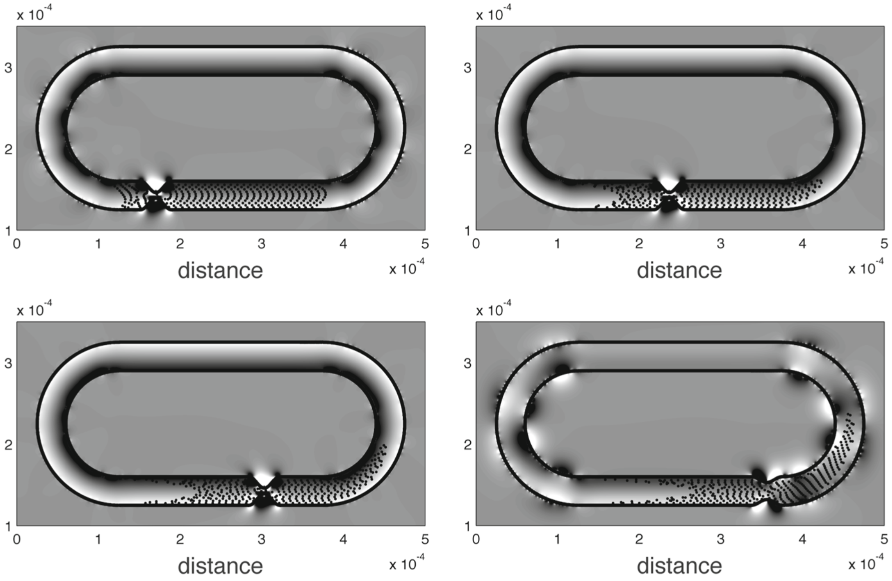

Fig. 6 Peristaltic pumping during the first pulse cycle at $t = \frac{\mathcal{T}}{4}, \frac{\mathcal{T}}{2}, \frac{3\mathcal{T}}{4}$, and $\mathcal{T}$. The Wo was set to 1.0 and the frequency was set to 1 Hz. The *graymap* shows the vorticity, and the *black dots* are passive tracers that move at the local fluid velocity

Significant net flow is produced in the positive (counterclockwise) direction. In the case of neuromechanical pumping, The flow rapidly accelerated during the initial contraction, exceeding the instantaneous speeds reached by the peristaltic mechanism. At

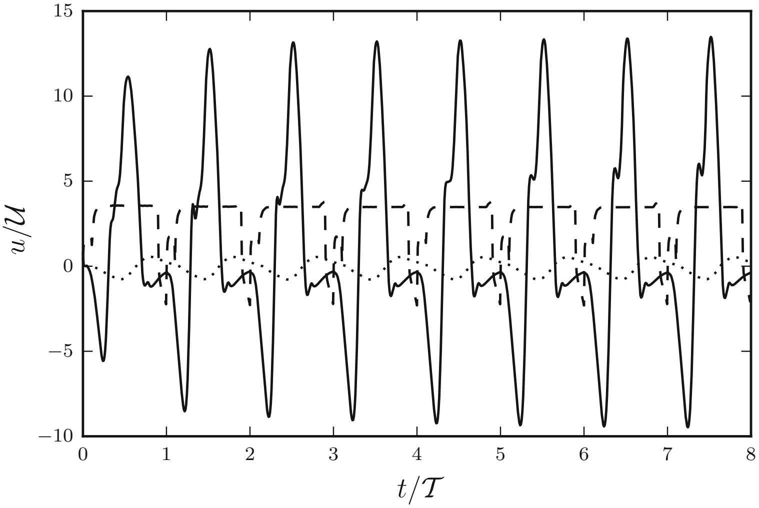

Fig. 7 Dimensionless spatially average flow velocity (u/U) versus dimensionless time ($t/\mathcal{T}$) at $f = 1.0$Hz and $Wo = 1.0$. *Solid line* neuromechanical suction pump, *dashed line* peristaltic pumping, *dotted line* dynamic suction pumping

the end of the pulse, some back flow is also produced. On average, the fluid is pushed in the positive (counterclockwise) direction.

The significant effect of viscous damping, that caused little net flow for the impedance pump, does not have the same effect for neuromechanical pumping and peristalsis. Compared to impedance pumping, neuromechanical pumping achieves higher maximum and lower minimum flow velocities. Neuromechanical pumping also produces higher bulk flow non-dimensional velocities ($u/\mathcal{U}$) 10, than impedance pumping, 1, see Fig. 7. Peristaltic pumping produces strong positive flows with little back flow, and the flow rapidly approaches a constant velocity during translation of the contraction site. Flow produced by neuromechanical pumping is more transient and unstable, not reaching a steady flow speed during the translation of the traveling wave down the tube that is characteristic of peristalsis. Maximum and minimum flow speeds are of greater magnitude than peristalsis. Bulk fluid movement is somewhat less for neuromechanical pumping compared to traditional peristalsis, 3 and 1 respectively, see Fig. 8.

3.3 Effect of Womersley number on flow rate

When Wo is set to 1, little flow is produced by impedance pumping given the significant amount of viscous damping and lack of passive traveling waves. To compare the performance of each of the pumps across a range of scales, Wo was varied from 0.3 to 16. This range includes the case where unsteady effects are negligible ($Wo = 0.3$) and the case where inertia is significant ($Wo = 16$). Figure 8 shows the dimensionless spatially and temporally average flow velocity (u/U) versus Wo. Both peristalsis and

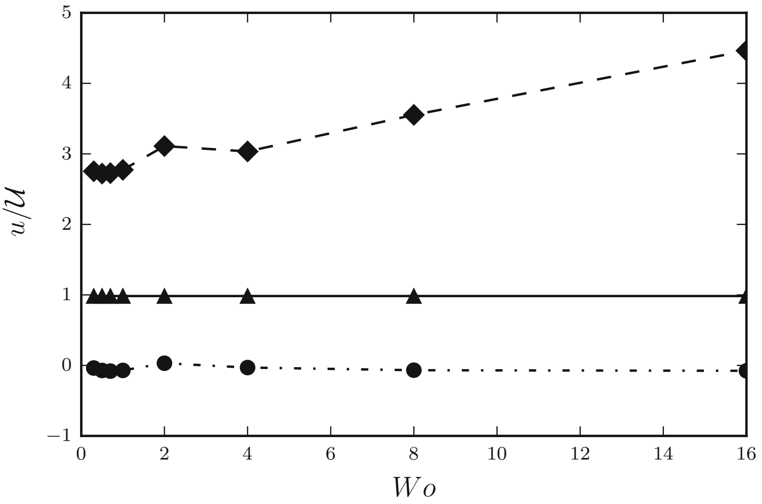

Fig. 8 Dimensionless spatially and temporally average flow velocity (u/U) versus Wo. *Solid line* neuromechanical suction pump, *dashed line* peristaltic pumping, and *dotted line* dynamic suction pumping. *Markers* indicate temporally averaged simulations for various Womersley numbers

neuromechanical pumping produce strong positive (counterclockwise) flows across the range of Wo, around 3 and 1 diameters per beat, respectively. Net flow is reduced for the lower Wo for peristalsis given the significant viscous resistance. Impedance pumping produces clockwise flow for most Wo, although bi-directional flow is characteristic of impedance pumping dependent upon Wo, frequency, and location of actuation site. For this choice of geometry and elastic properties, mostly clockwise flow is achieved with the exception of $Wo = 2$ where max counterclockwise flow is reached. It is worthwhile to note that impedance pumping can produce strong flows for $Wo >> 1$ for some choices of parameters [3,8,10].

3.4 Effect of pumping frequency on flow rate

One of the main characteristics of impedance pumping is the nonlinear relationship between frequency and flow [3,8]. For a given choice of geometry and elasticity of the tube, peaks in net flow can be seen at certain frequencies while changes in flow direction may be observed for other choices of frequency [10]. For the case of peristalsis, the relationship between frequency and flow is linear assuming that the wave speed changes in proportion to the pumping frequency [6]. If pumping frequency and wave speed are decoupled, leading to different waveforms as the frequency is varied, the relationship between frequency and flow may be nonlinear [30].

To determine whether or not a nonlinear frequency-flow relationship exists for the neuromechanical pumping mechanism presented in this paper, we performed the following simulations: (1) pumping frequency was varied from 0.3 to 2.2 Hz while the conduction velocity of the action potential used to initiate contraction was varied proportionally; and (2) the pumping frequency was varied but the conduction velocity

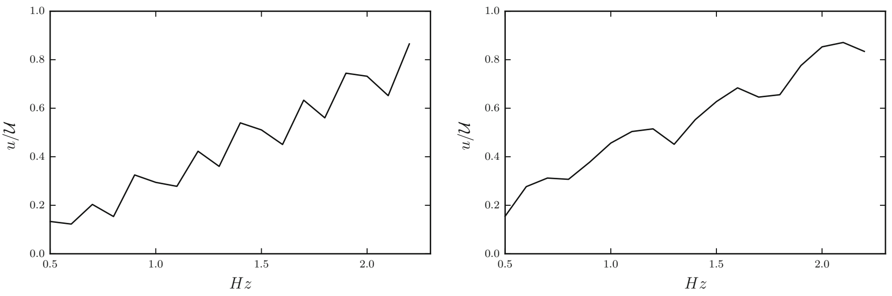

Fig. 9 Average dimensionless fluid velocity vs. pumping frequency for the neuromechanical pump. *Left* the wave speed changes proportionally with the pumping frequency. Translational compression wave travels the length of the elastic tube before the next compression begins. *Right* constant wave speed. The compression wave speed stays constant regardless of the frequency of the pacemaker. At high pumping frequencies, a new contraction is initiated before the prior contraction wave finishes

of the action potential was held constant. In the first case, the compression wave travels the length of the elastic tube before the next compression begins. In the second case, a new contraction may be initiated before (high frequencies) or well after (low frequencies) the prior contraction wave has finished. The results of these simulations are given in Fig. 9. Both graphs show the spatial and temporally averaged flow speeds as a function of the pumping frequency. Note that in both cases one can observe a nonlinear relationship between frequency and flow. Unlike the case of impedance pumping, however, the net flow is always in the positive (counterclockwise) direction.

4 Conclusions

In this paper, we present a neuromechanical model to describe pumping in an idealized tunicate heart. The scale (described here using the Womersley number, Wo) was matched to a typical heart of the tunicate *Ciona savignyi*. The neuromechanical model produced significant flows that share some of the main characteristics that have been described in tubular hearts: (1) a nonlinear relationship between heartbeat frequency and flow; (2) peak flows that exceed the wave speed; and (3) a bidirectional wave of contraction that emanates from the pacemaker region. We also note that the neuromechanical model that includes elastic deformations that emerge from the fluid-structure coupling generate more complicated kinematics than that of a simple prescribed contraction wave.

In the debate surrounding the pumping mechanisms of tubular, valveless hearts, it has been observed that the kinematics and flow produced by many tubular hearts resemble those produced by impedance pumping [6]. Our results show that similar dynamics may also be observed using a traveling wave of active contraction along an elastic tube. When evaluating possible pumping mechanisms, it is important to consider the specific geometry, scale, and elastic properties of the heart. For the parameters considered here, impedance pumping did not produce significant net flow. Interestingly, a prescribed peristaltic wave of contraction produced the strongest flow of all mechanisms considered. This is due to the fact that our neuromechanical model generated significant back flow between each contraction.

Based on the definition of a peristaltic pump typically used in the biological literature whereby flow is generated by a traveling wave of contraction, one might consider the neuromechanical pump presented here as a way to model peristalsis. It is important to note, however, that the neuromechanical pump includes a bidirectional wave of active contraction that is not a typical feature of peristaltic pumps. In addition, some of the motion of the elastic tube is due to the interaction of the elastic boundary with the fluid and the relatively rigid inflow and outflow tracts. One could argue that the resulting kinematics and flows are influenced to some degree by the Libeau mechanism that drives fluid in dynamic suction pumping. For our purposes, we will simply describe the neuromechanical pumping mechanism as it is implemented: a bidirectional wave of active tension imposed on an elastic tube.

Acknowledgments The authors would like to thank the Japanese Society for Mathematical Biology and the Society of Mathematical Biology for their support to attend the conference. This work was funded by NSF DMS CAREER # 1151478 awarded to L. A. M. and NSF DMS RTG # 0943851 to R. McLaughlin.

References

1. Anderson, M.: Electrophysiological studies on initiation and reversal of the heart beat in *Ciona intestinalis*. J. Exp. Biol. **49**, 363–385 (1968)
2. Baird, A., King, T., Miller, L.A.: Numerical study of scaling effects in peristalsis and dynamic suction pumping. In: Proceedings of the AMS, Special Session on Biological Fluid Dynamics: Modeling, Computations, and Applications, vol. 628, pp. 129–148 (2014)
3. Bringley, T., Childress, S., Vandenberghe, N., Zhang, J.: An experimental investigation and a simple model of a valveless pump. Phys. Fluids **20**(033), 602 (2008)
4. Davidson, B.: *Ciona intestinalis* as a model for cardiac development. Semin. Cell Dev. Biol. **18**, 16–26 (2007)
5. FitzHugh, R.: Impulses and physiological states in theoretical models of nerve membrane. Biophys. J. **1**(6), 445–466 (1961)
6. Forouhar, A.S., Liebling, M., Hickerson, A., Nasiraei-Moghaddam, A., Tsai, H., Hove, J.R., Fraser, S.E., Dickinson, M.E., Gharib, M.: The embryonic vertebrate heart tube is a dynamic suction pump. Science **312**(5774), 751–753 (2006). doi:10.1126/science.1123775. http://www.sciencemag.org/content/312/5774/751.abstract. http://www.sciencemag.org/content/312/5774/751.full.pdf
7. Harrison, J., Waters, J., Cease, A., Cease, A., VandenBrooks, J., Callier, V., Klok, C., Shaffer, K., Socha, J.: How locusts breathe. Physiology **28**, 18–27 (2013)
8. Hickerson, A.I., Rinderknecht, D., Gharib, M.: Experimental study of the behavior of a valveless impedance pump. Exp. Fluids **38**(4), 534–540 (2005)
9. Hodgkin, A.L., Huxley, A.F.: Propagation of electrical signals along giant nerve fibres. In: Proceedings of the Royal Society of London Series B, Biological Sciences, pp. 177–183 (1952)
10. Jung, E., Peskin, C.: Two-dimensional simulations of valveless pumping using the immersed boundary method. SIAM J. Sci. Comput. **23**(1), 19–45 (2001). doi:10.1137/S1064827500366094. http://epubs.siam.org/doi/abs/10.1137/S1064827500366094. http://epubs.siam.org/doi/pdf/10.1137/S1064827500366094
11. Kalk, M.: The organization of a tunicate heart. Tissue Cell **2**, 99–118 (1970)
12. Keener, J.P.: Wave propagation in Myocardium. In: Glass, L., Hunter, P., McCulloch, A. (eds.) Theory of Heart –Biomechanics, Biophysics, and Nonlinear Dynamics of Cardiac Function, pp. 405–436. Springer, New York (1991)
13. Kriebel, M.E.: Conduction velocity and intracellular action potentials of the tunicate heart. J. Gen. Physiol. **50**(8), 2097–2107 (1967)

14. Lemaire, P.: Evolutionary crossroads in developmental biology: the tunicates. Development **138**, 2143–2152 (2011)
15. Liebau, G.: Über ein ventilloses pumpprinzip. Naturwissenschaften **41**, 327–327 (1954). doi:10.1007/BF00644490
16. Liebau, G.: Die stromungsprinzipien des herzens. Z Kreislaufforsch **44**, 677 (1955)
17. Männer, J., Wessel, A., Yelbuz, T.: How does the tubular embryonic heart work? looking for the physical mechanism generating unidirectional blood flow in the valveless embryonic heart tube. Dev. Dyn. **239**, 1035–1046 (2010)
18. McMahon, B., Wilkens, J., Smith, P.: Invertebrate circulatory systems. Compr. Physiol. Suppl. **30**, 931–1008 (2011)
19. Miller, L.A., Peskin, C.S.: Flexible clap and fling in tiny insect flight. J. Exp. Biol. **212**(19), 3076–3090 (2009)
20. Mittal, R.: Locomotion with flexible propulsors: Ii. Computational modeling of pectoral fin swimming in sunfish. Bioinspir. Biomim. **1**, S35–S41 (2006)
21. Nichols, D.: The water-vascular system in living and fossil echinoderms. Palaeontology **15**(4), 519–538 (1972)
22. Pendar, H., Kenny, M.C., Socha, J.J.: Tracheal compression in pupae of the beetle zophobas morio. Biol. Lett. **11**(6), 20150,259 (2015)
23. Peskin, C.S.: The immersed boundary method. Acta Numer. **11**, 479–517 (2002). doi:10.1017/S0962492902000077. http://journals.cambridge.org/article_S0962492902000077
24. Peskin, C.S., McQueen, D.M.: Fluid dynamics of the heart and its valves. In: Othmer, H.G., Adler, F.R., Lewis, M.A., Dallon, J.C. (eds.) Case Studies in Mathematical Modeling: Ecology, Physiology, and Cell Biology, 2nd edn. Prentice-Hall, New Jersey (1996)
25. Pozrikidis, C.: A study of peristaltic flow. J. Fluid Mech. **180**, 515–527 (1987)
26. Socha, J.J., Lee, W.K., Harrison, J.F., Waters, J.S., Fezzaa, K., Westneat, M.W.: Correlated patterns of tracheal compression and convective gas exchange in a carabid beetle. J. Exp. Biol. **211**(21), 3409–3420 (2008)
27. Teran, J., Fauci, L., Shelley, M.: Viscoelastic fluid response can increase the speed and efficiency of a free swimmer. Phys. Rev. Lett. **104**(3), 38,101 (2010)
28. Tytell, E.D., Hsu, C., Williams, T.L., Cohen, A.H., Fauci, L.J.: Interactions between internal forces, body stiffness, and fluid environment in a neuromechanical model of lamprey swimming. Proc. Natl. Acad. Sci. **107**(46), 19,832–19,837 (2010)
29. Waldrop, L., Miller, L.: The role of the pericardium in the valveless, tubular heart of the tunicate, ciona savignyi. J. Exp. Biol. **218**, 2753–2763 (2015a). doi:10.1242/jeb.116863
30. Waldrop, L., Miller, L.A.: Large-amplitude, short-wave peristalsis and its implications for transport. Biomech. Model. Mechanobiol. (2015b). doi:10.1007/s10237-015-0713
31. Xavier-Neto, J., Castro, R., Sampaio, A., Azambuja, A., Castillo, H., Cravo, R., Simoes-Costa, M.: Parallel avenues in the evolution of hearts and pumping organs. Cell. Mol. Life Sci. **64**, 719–734 (2007)
32. Xavier-Neto, J., Davidson, B., Simoes-Costa, M., Castillo, H., Sampaio, A., Azambuja, A.: Evolutionary origins of the heart. In: Rosenthal, N., Harvey, R. (eds.) Heart Development and Regeneration, vol. 1, 1st edn, pp. 3–38. Elsevier Science and Technology, London (2010)